Hindawi
Advances in Materials Science and Engineering
Volume 2022, Article ID 6278342, 11 pages
https://doi.org/10.1155/2022/6278342

Research Article

Experimental and Thermodynamic Investigation on CO_2 Absorption in Aqueous MEA Solutions

Kai Zhu,[1] Changhai Yue,[1] Zhenhao Wei,[1] Jingjing Huang,[1] Meng Hu,[1] Yufan Ji,[1] Hanfei Liu,[1] Hao Zhu,[1] Wanxiao Guo,[1] Feng Zhou,[2] Chaoqun Yao,[3] and Yiping Huang[1]

[1]*China Construction Industrial & Energy Engineering Group Co., Ltd., 6, Wenlan Road, Qixia District, Nanjing, 210023, China*
[2]*National & Local Joint Engineering Research Center for Deep Utilization Technology of Rock-salt Resource, Faculty of Chemical Engineering, Huaiyin Institute of Technology, Huai'an 223003, China*
[3]*Dalian National Laboratory for Clean Energy, Dalian Institute of Chemical Physics, Chinese Academy of Sciences, Dalian 116023, China*

Correspondence should be addressed to Feng Zhou; zhoufeng@hyit.edu.cn and Yiping Huang; huangyiping@cscec.com

Received 24 June 2022; Accepted 23 August 2022; Published 13 October 2022

Academic Editor: Ghulam Rasool

The vapor-liquid equilibrium (VLE) of CO_2 in a reactive solvent is essential for the proper simulation and design of CO_2 absorption processes. This work presents a systematic investigation on CO_2 absorption in various aqueous monoethanolamine (MEA) solutions. CO_2 solubility in MEA was measured at 298, 313, 333, and 353 K with CO_2 partial pressure ranging from 34.5 to 78.0 kPa. A modified Kent-Eisenberg model was developed based on the measured solubility data, showing good predictions over the liquid phase speciation for the CO_2-H_2O-MEA system. We presented a new analysis based on the first-order difference curve of distribution profiles of the species. Based on the main reactions that occurred, the CO_2 absorption process was demonstrated to be divided into four regions with increasing CO_2 loading from 0 to 1. Accordingly, kinetic study was proposed to be conducted in the first region, whereas measuring of mass transfer in the first three regions. The findings in this work extend the existing knowledge of CO_2 absorption process in terms of speciation and can provide important guidance for further study of the process characteristics using aqueous amine absorbents.

1. Introduction

Since industrial activities have expanded over the past several decades, global warming and climate change have become increasingly important environmental issues in the twenty-first century (Reference [1]). Carbon dioxide (CO_2), as a greenhouse gas, mainly from large point sources, such as coal-based power plant and refinery off-gases, is the main contributor to the global warming and climate changes. Therefore, developing efficient technologies to capture and separate CO_2 is becoming increasingly popular. Chemical absorption with alkanolamines is the most suitable technique currently available for CO_2 removal [2–6]. Monoethanolamine (MEA), as a primary amine, is under intense research because of its various advantages, such as high chemical reactivity with CO_2, low cost of materials, and ease of production [7–11]. However, the application of this system is hindered by its large energy requirement in the regeneration process [12, 13], which reduces the output of a coal-fired power plant by 30-40% [14, 15].

Understanding the fundamentals of absorption/desorption deeply, including thermodynamics, kinetics, and mass transfer, is essential for dealing with the problem of extensive energy consumption; (Reference [16]). The thermodynamic properties play a pivotal role in the design and optimization of CO_2 capture processes, involving vapor-liquid equilibrium (VLE), solubility, enthalpy, as well as equilibrium speciation. As a result, a great deal of effort has been put into the determination of the thermodynamic properties of CO_2 absorption into MEA solution and the development of thermodynamic models to describe them. Mouhoubi et al. [17] developed a thermodynamic model for

the carbon capture process of DEEA, MAPA, and their mixtures, in which experimental data from the literature were compared favorably with the predicted and correlated data of vapor-liquid equilibrium (VLE) and heat of CO_2 absorption. Ma'mun et al. [18] measured the protonation constant of MEA at a range of temperatures from 303 to 330 K and presented an empirical equation correlating the influence of temperature. Aronu et al. [19] reported a series of CO_2 solubility data for MEA, along with a rigorous equilibrium model that fits the experimental VLE data well. Ojala et al. [20] measured the absorption enthalpy and compared to predictive models in the literature, showing a high level of agreement. Additionally, as there are several reversible chemical reactions, it is necessary to study the speciation of the liquid mixture, which not only has an essential influence on the VLE [21] but is also indispensable for simulation models coupling mass transfer [19, 22].

Chemical speciation in the absorption system can be obtained by experimental measurement [23–26], thermodynamic model prediction [12, 19, 21, 27, 28], or molecular simulations [29]. Jakobsen et al. [23] and Bottinger et al. [24] showed that nuclear magnetic resonance (NMR) spectroscopy was capable of acquiring quantitative information on the species distribution, but unable to distinguish the protonated and unprotonated amines. Wong et al. [25], however, showed that Raman spectroscopy could give a clear distribution of all species in CO_2-loaded MEA solutions. In Li's research, for the CO_2 capture system using aqueous HEPZ, the cyclic capacity, speciation with loading, and heat of reaction are predicted and analyzed using the developed thermodynamic model. [30] A simple VLE model based on Henry's law and equilibrium of eight reversible reactions was proposed by Kent and Eisenberg [28] ignoring the activity coefficients to predict equilibrium compositions. As compared with NMR data, Hessen et al. [12] demonstrated that the refined electrolyte nonrandom two liquid (NRTL) model could give a good prediction of the speciation. Using Helmholtz energy equations of state combined with excess Gibbs energy models, Neumann et al. [31] formulated a model for describing reactive mixtures that reproduced experimental data of vapor-liquid equilibrium, homogeneous density, and speciation of partial binary/ternary systems involving monoethanolamine well. As reported by Balaji et al. [29], accurate species concentrations could only be obtained through molecular simulations in which bicarbonate hydrolysis is included in the reaction pathway when loadings exceed 0.5 mol CO_2/mol MEA, but it can be neglected in cases where CO_2 loadings are lower than 0.5 mol CO2/mol MEA.

In spite of the relatively large number of publications concerned with chemical speciation in the MEA system, all of these studies only reported species distribution profiles and did not provide detailed analyses of the evolution rate of the species under varying CO_2 loads. In our work, CO_2 solubility in MEA aqueous solution was examined at temperatures ranging from 298 to 353 K and CO_2 partial pressures ranging from 34.5 to 78.0 kPa. Based on Kent-Eisenberg model framework [28], a modified model was developed using measured solubility data. Based on the obtained thermodynamic model, the species distributions of a 20 wt.% MEA system under different CO_2 loadings are well predicted. The first-order difference curve of species distribution profiles was derived as a new approach to analyzing the absorption process. Therefore, four speciation regions were first proposed based on the usage of a first-order difference method dealing the equilibrium concentration. It is noteworthy that the results obtained in this work not only contribute to the existing knowledge regarding speciation of CO_2 absorption process but also provide a basis for further study of the characteristics of aqueous amine absorption processes.

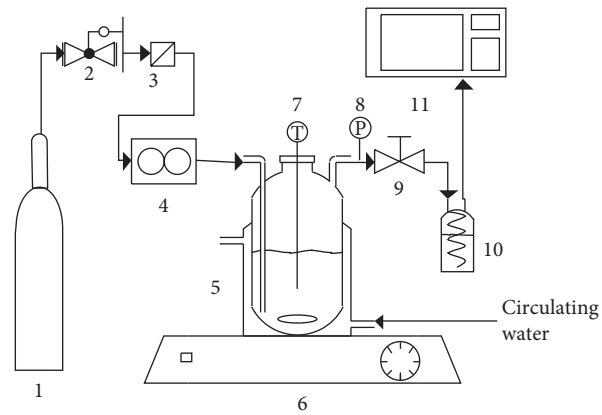

Figure 1: Schematic of the experimental setup for measuring CO_2 solubility. 1: High pressure gas cylinder, 2: pressure regulator valve, 3: filter, 4: mass control flowmeter, 5: equilibrium cell, 6: magnetic stirrer, 7: temperature sensor, 8: pressure sensor, 9: backpressure valve, 10: silica gel dryer, and 11: gas chromatography.

2. Materials and Methods

2.1. Reagents. Monoethanolamine (MEA) with a mass fraction purity of >99% was supplied by Kermel Co. Ltd. 20 wt.% (3.285 mol/L) aqueous MEA solution was prepared by mixing amine and deionized water. 30 vol.% carbon dioxide (CO_2) balanced with nitrogen (N_2) was supplied by Dalian Special Gas Co. Ltd.

2.2. Measurement of Solubility of CO_2. The solubility of CO_2 was measured using the experimental setup shown in Figure 1. The equilibrium cell with an inner volume of 130 ml was made up of stainless steel. A water circulating bath was used to control the temperature of the equilibrium cell. A magnetic stirrer was placed under the equilibrium cell to maintain a constant stirring speed of the absorption solution. A mass flow controller (0-500 mL/min of N_2 at 0°C, 101.325 kPa) was used to deliver the gas mixture at a constant flow rate. A back pressure valve and pressure sensor were used to maintain the outlet pressure of the equilibrium cell at the required pressure. A gas chromatography (GC) was used to measure the CO_2 concentration of the outlet gas after absorption as shown in Figure 1. A CarboPLOT-P7 column (12.5 m × 530 μ m× 20μ m, Agilent) and thermal conductivity detector (TCD) were installed in the GC. The

temperature of the column and TCD were set at 303 and 523K, respectively. All the experiments were carried out over a temperature range of 298 to 353 K and a CO_2 partial pressure range of 34.5 to 78.0 kPa. The total amount of CO_2 dissolved in the absorbent was calculated by integrating differences between the concentrations of injected CO_2 and emitted CO_2. The amounts of CO_2 injected into the tank and emitted from the tank were calculated by the ideal gas equation. Thus, the CO_2 dissolved in the absorbent can be determined through equation (1). CO_2 loading (α), defined as the ratio of mole of absorbed CO_2 to mole of absorbent, can be calculated using equation (2).

$$n_{co_2,abs} = \frac{p}{RT}\int \left(Q_{in}C_{in} - Q_{out}C_{out}\right)_{dt}, \tag{1}$$

$$\alpha = \frac{n_{co_{2,abs}}}{n_{MEA}}. \tag{2}$$

2.3. Thermodynamic Framework. In order to understand the chemical speciation in the solution with increasing CO_2 loading, the bulk concentrations of species are required. Thus, the chemical reaction process, the vapor-liquid equilibrium model (VLE), and some model parameters are required as follows.

2.3.1. Chemical Reaction Process. In the absorption process of CO_2 into MEA [32–34], some species exist in the systems, including CO_2, H_2O, RNH_2, RNH+ 3, $RNHCOO^-$, H_3O^+, OH^-, HCO_3^-, and CO_3^{2-}. Reactions as follows may occur in the liquid phase [23, 24, 34].

Carbamate formation reaction:

$$\begin{aligned} CO_2 + 2RNH_2 &\overset{K1}{\rightleftarrows} K_1 RNH_3^+ + RNHCOO^- \\ CO_2 + RNH_2 + H_2O &\overset{K2}{\rightleftarrows} K_2 H_3O^+ + RNHCOO^- \\ CO_2 + RNH_2 + OH^- &\overset{K3}{\rightleftarrows} K_3 H_2O + RNHCOO^- \\ CO_2 + RNH_2 + CO_3^{2-} &\overset{K4}{\rightleftarrows} K_4 HCO_3^- + RNHCOO^- \end{aligned} \tag{3}$$

Water ionization reaction:

$$2H_2O \overset{k5}{\rightleftarrows} k_5 H_3O^+ + OH^-. \tag{4}$$

Dissociation reaction of dissolved CO_2:

$$CO_2 + 2H_2O \overset{K6}{\rightleftarrows} K_6 H_2O^+ + HCO_3^-. \tag{5}$$

Dissociation reaction of bicarbonate:

$$HCO_3^- + H_2O \overset{K7}{\rightleftarrows} K_7 CO_3^{2-} + H_3O^+. \tag{6}$$

Dissociation reaction of RNH_3^+:

$$RNH_3^+ + H_2O \overset{K8}{\rightleftarrows} K_8 RNH_2 + H_3O^+. \tag{7}$$

With the increase of CO_2 loading, the concentration of MEA in the solution gradually decreases, and the solution gradually becomes acidic. Meanwhile, the concentration of the protonated MEA gradually increases. Thus, the carbamate hydrolysis reaction, which was adopted by several research studies to form the equilibrium framework [27, 28, 33], is not involved to reflect the consumption of carbamate for relatively high CO_2 loading. Instead, equation (8) was used as a main modification to the model of Kent and Eisenberg [28]. A similar treatment was also adopted by Aboulheir [33] for the consumption of the zwitterion.

Carbamate consumption reaction:

$$RNHCOO^- + H_3O^+ \overset{K9}{\rightleftarrows} K_9 RNH_3^+ + HCO_3^-. \tag{8}$$

The above process consisting of some reactions allows us to understand the whole absorption process of CO_2 into the aqueous MEA solution.

2.3.2. Vapor-Liquid Equilibrium Model. In the present work, the vapor-liquid equilibrium is based on the physicochemical Kent-Eisenberg model [28]. Compared to the refined electrolyte NRTL model [12] and molecular simulations [29], the model that assumes all activity coefficients and fugacity coefficient to be unity in the solutions is relatively simple and has good performance in predicting the CO_2 solubility [28, 35–38]. It was essential to adjust it to the thermodynamics of our systems, in terms of balance equations and equilibrium constants. The chemical equilibrium in the system is governed by equations (4)-(8). The pseudo-equilibrium constants representing the reactions in the CO_2/MEA/H_2O system are given by equations (9)-(13).

$$K_5 = \left[H_3O^+\right]\left[OH^-\right] \tag{9}$$

$$K_6 = \left[H_3O^+\right]\left[\frac{HCO_3^-}{CO_2}\right] \tag{10}$$

$$K_7 = \left[H_3O^+\right]\left[\frac{CO_3^{2-}}{HCO_3^-}\right] \tag{11}$$

$$K_8 = \frac{\left[RNH_2\right]\left[H_3O^+\right]}{\left[RNH_3^+\right]} \tag{12}$$

$$K_9 = \frac{\left[RNH_3^+\right]\left[HCO_3^-\right]}{\left[RNHCOO^-\right]\left[H_3O^+\right]}. \tag{13}$$

In addition to the above equilibrium equations, the mass balance equations of amine and carbon dioxide (equations (14) and (15)) and charge balance equation (16) must be satisfied.

$$\left[RNH_2\right]_t = \left[RNH_2\right] + \left[RNH_3^+\right] + \left[RNHCOO^-\right] \tag{14}$$

$$\begin{aligned} \left[CO_2\right]_t &= \alpha\left[RNH_2\right]_t \\ &= \left[CO_2\right] + \left[HCO_3^-\right] + \left[CO_3^{2-}\right] + \left[RNHCOO^-\right]. \end{aligned} \tag{15}$$

$$\left[RNH_3^+\right] + \left[H_3O^+\right] = \left[OH^-\right] + \left[HCO_3^-\right] + 2\left[CO_3^{2-}\right] + \left[RNHCOO^-\right]. \tag{16}$$

The physically dissolved CO_2 concentration is related to the CO_2 equilibrium partial pressure in the solvent by Henry's law.

$$\left[CO_2\right] = \frac{p_{CO_2}}{H_{CO_2}}. \tag{17}$$

The nine equations, equations (9)-(17), may be solved to obtain the value of CO_2 loading over MEA solutions of a given CO_2 partial pressure at a particular temperature. Equations (9)-(17) can be reduced, and expressions about the CO_2 loading, α, and $[H^+]$ can be obtained consequently, shown in equations (18) and (19).

Table 1: Pseudo-equilibrium constants.

Equilibrium constant[a]	a_1	a_2	a_3
K_5, $(mol/L)^2$	−13445.9	−22.4773	140.932
K_6, (mol/L)	−12092.1	−36.7816	235.482
K_7, (mol/L)	−12431.7	−35.4819	220.067

[a]Correlation: $\ln K = a_1/T + a_2 \ln T + a_3$, T in K.

Table 2: CO_2 Henry's coefficients in 20 wt. % aqueous MEA solution.

Temperature, K	298	313	333	353
H_{CO2}, kPa/(kmol/m^3)	3251.62	4078.31	5344.08	6791.55

$$\alpha = \frac{\left(P_{CO_2}/H_{CO_2}\right) + \left(K_6 P_{CO_2}/H_{CO_2}[H^+]\right) + \left(K_6 K_7 P_{CO_2}/H_{CO_2}[H^+]^2\right) + \left(\left(K_6[RNH_2]_t P_{CO_2}/H_{CO_2}\right)/\left(K_8 K_9[H^+] + K_6 P_{CO_2}/H_{CO_2} + K_9[H^+]^2\right)\right)}{[RNH_2]_t}, \tag{18}$$

$$[H^+] = \frac{K_5}{[H^+]} + \frac{K_6 P_{CO_2}}{H_{CO_2}[H^+]} + 2\frac{K_6 K_7 P_{CO_2}}{H_{CO_2}[H^+]^2} + \frac{K_6[RNH_2]_t P_{CO_2}/H_{CO_2} - K_9[RNH_2]_t[H^+]^2}{K_8 K_9[H^+] + K_6 P_{CO_2}/H_{CO_2} + K_9[H^+]^2}. \tag{19}$$

For the above equation, values of K_5, K_6, and K_7 used in the calculation are obtained from the published literature [33], summarized in Table 1. H_{CO2} is the Henry's coefficients, which can be calculated by the correlation from Tsai et al. [39, 40], summarized in Table 2. Therefore, there are three parameters (K_8, K_9, and $[H^+]$) remaining unsolved. By fitting the equations to the experimental values of CO_2 loading and partial pressure for each temperature condition using Levenberg–Marquardt algorithm, we could obtain the parameters of K_8 and K_9. During fitting, the range of $[H^+]$ was limited between 10^{-6} and 10^{-12} mol/L [41]. After K_8 and K_9 were obtained, they were substituted into equations (9)-(17) to calculate the species equilibrium concentration, including $[H^+]$.

3. Result and Discussion

3.1. CO_2 Absorption Curve in MEA Absorbent. Figure 2 shows the absorption curves of CO_2 in an MEA aqueous solution at different temperatures. The absorption curve presents the ratios of CO_2 concentrations at the outlet gas (C_{out}) to the initial CO_2 concentration (C_{in}) as a function of time [42]. From the absorption curve at 298 K, it can be observed that C_{out}/C_{in} is close to zero in the first 35 minutes of the absorption process, and then increases rapidly thereafter. It can be speculated that most MEA has been consumed in the first 35 minutes. Due to the significantly lower MEA concentration, absorption rates decreased in the later phase. Absorption curves shift to the left as absorption temperature increases, indicating a faster saturation. Based on the absorption curve, the absorption load of MEA at different temperatures can be achieved through equation (1).

3.2. CO_2 Solubility. The solubility of CO_2 in 20 wt.% aqueous MEA solutions was investigated to determine the dissociation equilibrium constants (K_8) of the RNH+ 3 and the carbamate consumption equilibrium constants (K_9) at 298, 313, 333, and 353 K. The experimentally measured CO_2 loadings are plotted in Figure 3 for aqueous MEA solutions. The values of K_8 and K_9, which were obtained by using the modified Kent-Eisenberg model as discussed above and experimentally measured CO_2 loadings, are summarized in Table 3. According to the correlation equation of Table 1, constants a_1, a_2, and a_3 are, respectively,−5880.90, 0, and −3.24111 for K_8 and 3117.05, 0, and 8.94366 for K_9.

In Figure 3, we present the experimental CO_2 solubility as well as a comparison with the prediction of the modified Kent-Eisenberg model for various CO_2 loadings and temperatures. To facilitate comparison, experimental data from Wong et al. [25] and Lee et al. [43] are also included. It is evident that the new model is capable of correlating all the CO_2 solubility data well over the temperature range

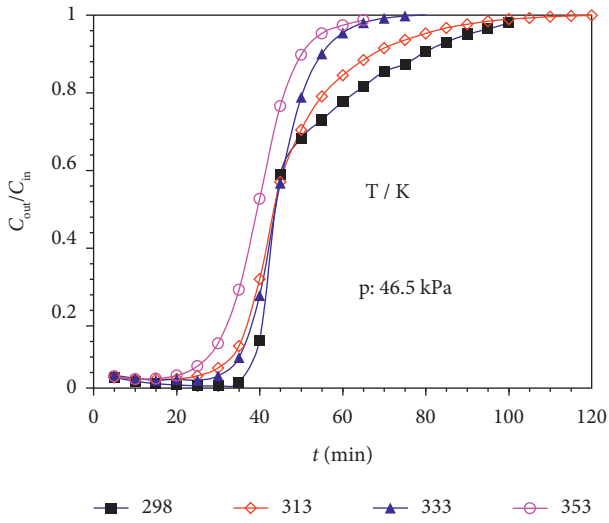

Figure 2: CO_2 absorption curves of MEA with 20wt.%.

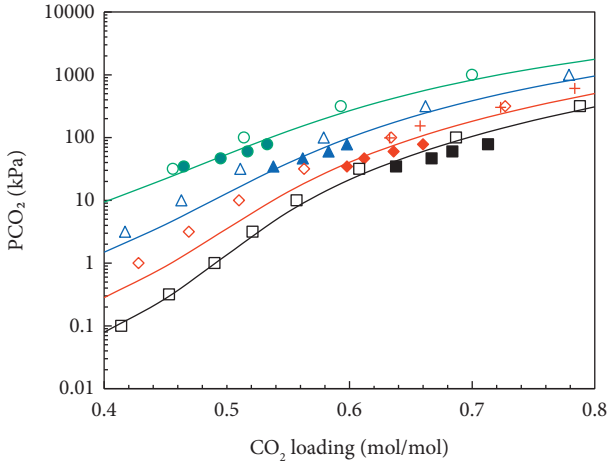

Figure 3: Comparison of the experimental data (symbols) for CO_2 partial pressure of MEA-H_2O-CO_2 system and the model results (lines), 20 wt.% MEA. Full symbols: experimental data from this work; +–313K, Wong et al. [25]; □–298 K, ◇-313K, Δ–333 K, ○–353K Lee et al. [43].

Table 3: Values of K_8 and K_9 in 20 wt. % aqueous MEA solution.

Temperature, K	K_8, (mol/L)	K_9, $(mol/L)^0$
298	$1.09693E-10$	$2.66631E+08$
313	$2.63471E-10$	$1.62296E+08$
333	$7.78297E-10$	$8.90972E+07$
353	$2.40987E-09$	$5.22888E+07$

considered. Figure 4 illustrates the overall comparison of experimental equilibrium solubility data and values correlated from the modified Kent-Eisenberg model. As shown in the parity plot, all data points fall within 5% relative deviation, indicating a high degree of accuracy and reliability.

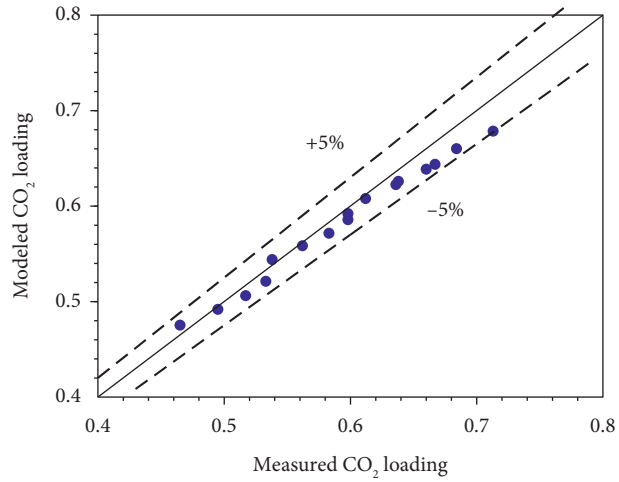

Figure 4: Parity plot of CO_2 solubility in aqueous MEA from 298 to 353 K obtained from experimental measurement and modified Kent-Eisenberg model prediction.

3.3. Chemical Species Distribution. The concentration distribution of liquid-phase species was analyzed with the modified Kent-Eisenberg model. Figure 5(a) shows a typical distribution profile at 313 K as a function of CO_2 loading, which is similar to the widely reported profile of CO_2 in primary amines. It is noteworthy that the equilibrium concentrations of CO_3^{2-}, OH^-, and H_3O^+ are very low and almost unchanged with the increase of loading from 0 to 1.0 mol CO_2/mol MEA. Thus, CO_3^{2-}, OH^-, and H_3O^+ were neglected in the whole absorption process, which is consistent with a previous study [24]. The modeled speciation results are compared with experimental results of NMR-spectroscopic measurements from Bottinger et al. [24] and Raman-spectroscopic measurements from Wong et al. [25]. Since protonated and unprotonated amines cannot be distinguished in NMR experiments, only HCO_3^- and $RNHCOO^-$ from Bottinger et al. [24] are shown for comparison. As can be seen in Figure 5(a), model predictions are in a good agreement with literature NMR and Raman data at low loading levels, whereas slight deviations are observed at high loading levels, likely due to the increased experimental uncertainty at these levels [21]. Similar deviations are observed in the literature as well [24, 25]. In addition, the modified Kent-Eisenberg model developed in this work generally gives better predictions than the previously reported Deshmukh–Mather model especially at high loadings [25, 44]. In general, the developed model displays a very good agreement with the experimental data obtained, either from NMR or Raman spectroscopy measurements, demonstrating its robustness.

For better understanding of the absorption process, the first-order difference curve of the equilibrium concentrations of all the species as a function of CO_2 loading with a difference step of 0.02 was further derived, as shown in Figure 5(b). Four regions are distinguished:

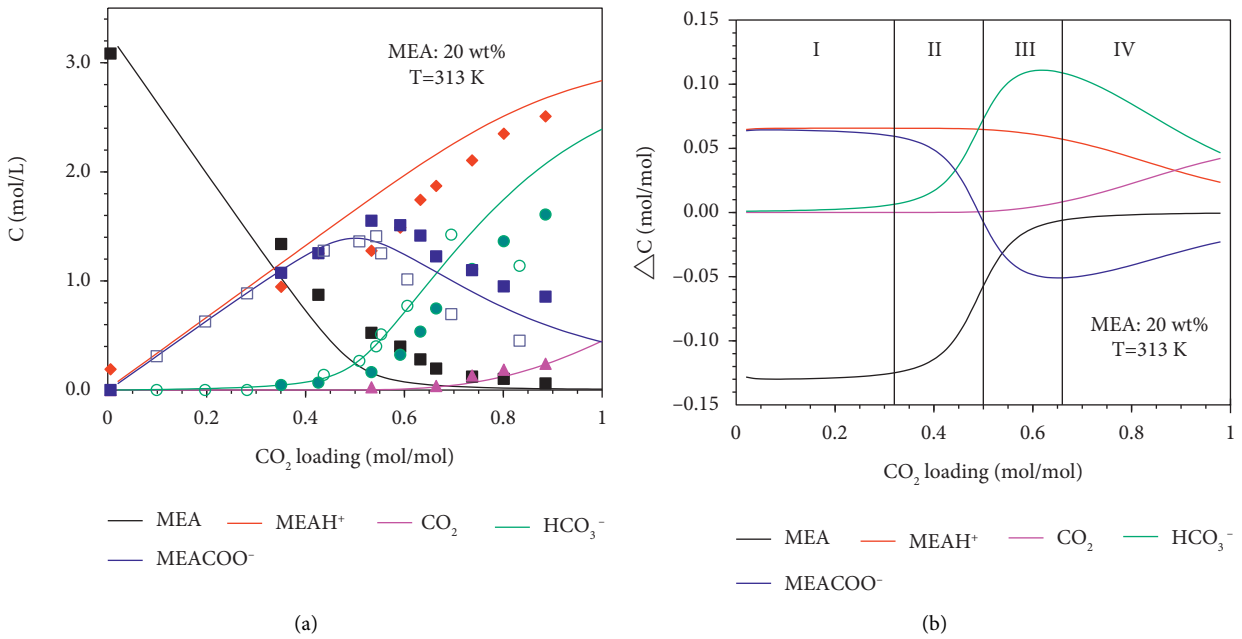

FIGURE 5: (a) Equilibrium speciation in MEA aqueous solution as a function of CO_2 loading. (b) First-order difference curve of equilibrium speciation as a function of CO_2 loading. Lines: data from modified Kent-Eisenberg model prediction; full symbols: experimental data of Wong et al. [25]; and empty symbols: experimental data of Bottinger et al. [24].

TABLE 4: Four regions of CO_2 absorption in MEA with CO_2 loading from 0 to 1 at 313 K.

Region	CO_2 loading	Main reaction processes
I	0-0.32	$CO_2 + 2H_2O \overset{K6}{\rightleftarrows} K_6 H_2O^+ + HCO_3^-$ (3)
II[a]	0.32-0.5	$CO_2 + 2RNH_2 \overset{K1}{\rightleftarrows} K_1 RNH_3^+ + RNHCOO^-$ (3) $CO_2 + 2H_2O \overset{K6}{\rightleftarrows} K_6 H_2O^+ + HCO_3^-$ (5) $RNHCOO^- + H_3O^+ \overset{K9}{\rightleftarrows} K_9 RNH_3^+ + HCO_3^-$ (8)
III[b]	0.5-0.66	$CO_2 + 2RNH_2 \overset{K1}{\rightleftarrows} K_1 RNH_3^+ + RNHCOO^-$ (3) $CO_2 + 2H_2O \overset{K6}{\rightleftarrows} K_6 H_2O^+ + HCO_3^-$ (5) $RNHCOO^- + H_3O^+ \overset{K9}{\rightleftarrows} K_9 RNH_3^+ + HCO_3^-$ (8)
IV	0.66-1	$CO_2 + 2H_2O \overset{K6}{\rightleftarrows} K_6 H_2O^+ + HCO_3^-$ (5) $RNHCOO^- + H_3O^+ \overset{K9}{\rightleftarrows} K_9 RNH_3^+ + HCO_3^-$ (8)

[a]In region II, equation (3) is the dominant reaction. [b] In region III, equations (5) and (8) are the dominant reactions.

(1) When CO_2 loading is less than 0.32 mol CO_2/mol MEA, CO_2 dissolved in the aqueous MEA solution is all converted into carbamate. The ratio of the difference values of MEA, RNH+ 3, and $RNHCOO^-$ (−2 : 1 : 1) obeys the stoichiometric ratio of Reaction (3), and this reaction is the major process while other reactions can be neglected in the absorption process.

(2) For CO_2 loading in the range of 0.32-0.5 mol CO_2/mol MEA, the difference value of $RNHCOO^-$ concentration decreases significantly. It implies that Reaction (8) begins to take place and consumes the $RNHCOO^-$ formed by Reaction (3). As the difference value of $RNHCOO^-$ is still positive, Reaction (3) dominates over Reaction (8). In this region, CO_2 hydrolysis (Reaction (5)) also occurs since it provides H_3O^+ for $RNHCOO^-$ consumption.

(3) For the CO_2 loading between 0.5 and 0.66 mol CO_2/mol MEA, the difference value of $RNHCOO^-$ begins to be negative, namely, the equilibrium concentration of $RNHCOO^-$ begins to decrease. Meanwhile, MEA is still present in the solution as shown in Figure 5(a) and $RNHCOO^-$ is formed continuously. Thus, in this region, Reactions (3), (5), and (8) all occur, but the latter two reactions are dominant. Due to that both Reactions (3) and (8) generate RNH_3^+, and the difference value of RNH_3^+ equilibrium concentration keeps almost unchanged in the first three regions from 0 to 0.66 mol CO_2/mol MEA.

(4) For the loading from 0.66 to 1 mol CO_2/mol MEA, only the consumption reaction of $RNHCOO^-$(Reaction (8)) and CO_2 hydrolysis reaction take place. MEA has been completely consumed and no $RNHCOO^-$ forms any more, leading to a minimum difference value of $RNHCOO^-$ at the CO_2 loading of 0.66 CO_2/mol MEA. Meanwhile, the difference value of CO_2 concentration begins to increase significantly in this region, indicating a declined CO_2 hydrolysis reaction. This then leads to declined $RNHCOO^-$ consumption, that is, decreased

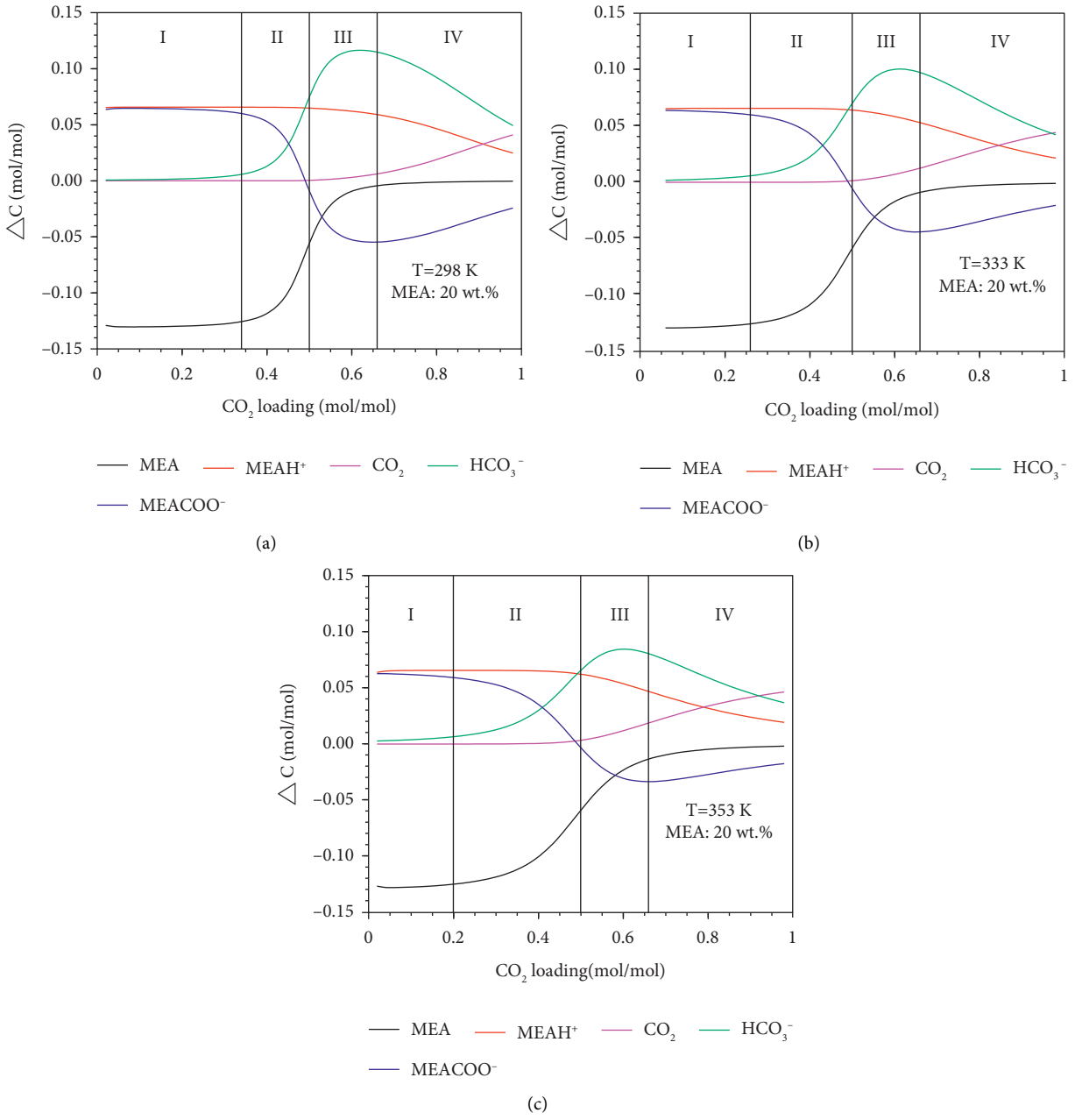

Figure 6: First-order difference curve of equilibrium speciation as a function of CO_2 loading at different temperatures (a) $T = 298$ K; (b) $T = 333$ K; and (c) $T = 353$ K.

Table 5: Four regions of CO_2 absorption in MEA with CO_2 loading from 0 to 1 at different temperatures.

T/K	Region			
	I	II	III	IV
298	0-0.34	0.34-0.5	0.5-0.66	0.66-1
313	0-0.32	0.32-0.5	0.5-0.66	0.66-1
333	0-0.26	0.26-0.5	0.5-0.66	0.66-1
353	0-0.2	0.2-0.5	0.5-0.66	0.66-1

evolution rates (absolute difference values) of $RNHCOO^-$ and RNH_3^+ equilibrium concentration, as shown in Figure 5(b). This is also consistent with the decreased difference value of HCO_3^- as the product of Reaction (8).

The four regions and main reactions are summarized in Table 4. In most of the previous studies, the process was simply divided into two regions at the point of 0.5 CO_2/mol MEA [24, 25, 29], which is the first time the process has been divided into four regions based on analyzing the difference curve of speciation. The first-order difference curve provides a better understanding over the equilibrium reactions. As can be seen from Table 4, the first region involves only one reaction, whereas the other three regions involve multiple reactions. Based on this, kinetic study of CO_2 absorption process should be conducted in the first region. In light of

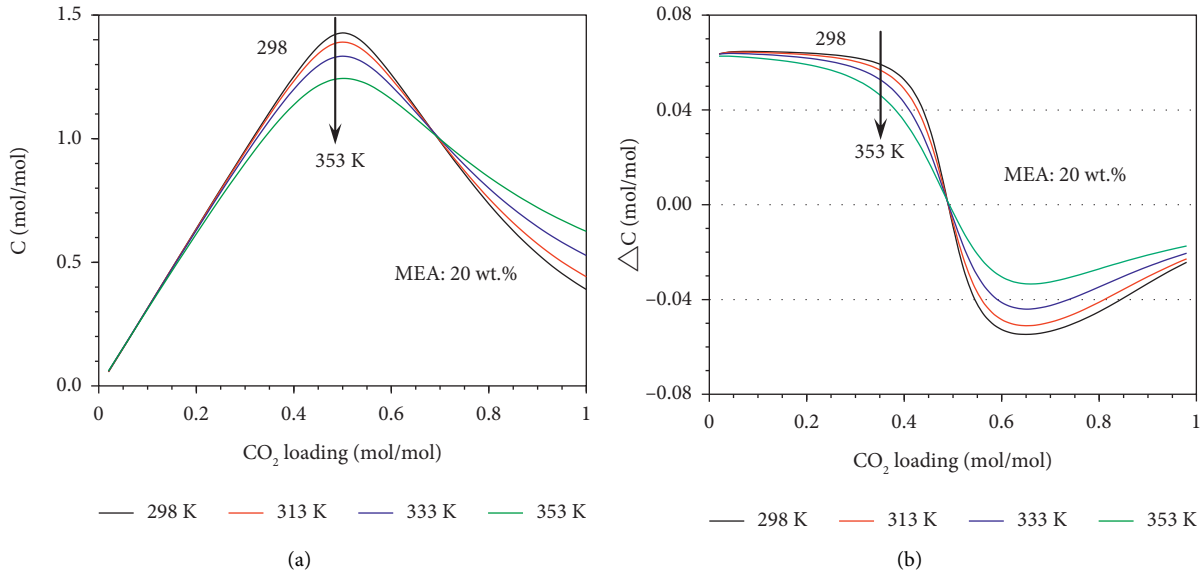

Figure 7: (a) $RNHCOO^-$ equilibrium concentrations at different temperatures as a function of CO_2 loading. (b) First-order difference curve of $RNHCOO^-$ equilibrium concentrations as a function of CO_2 loading.

the fact that the bulk CO_2 equilibrium concentration increases very significantly in the fourth region, mass transfer measurement should be conducted in the first three regions rather than in the fourth.

The equilibrium species profile and the corresponding first-order difference curve of CO_2/MEA system at different temperatures of 298, 333, and 353 K are also investigated, as shown in Figure 6. It can be observed that an increase in temperature does not significantly affect the trends described above, which is in consistent with the literature. Bottinger et al. [24] compared the results of the species concentrations at 293 and 333 K, showing a very weak dependence with temperature. Balaji et al. [29] also found a similar phenomenon for results of the speciation at 333 and 353 K. For all studied temperatures, CO_2 absorption process can also be divided into four regions at different temperatures. Whereas, the critical point between regions I and II changes notably with temperature. As shown in Table 5, the critical CO_2 loading between regions I and II becomes lower at higher temperatures. However, other critical points show no obvious change with temperature.

3.4. Effect of Temperature on Equilibrium Concentrations. Considering carbamate to be the most important species in CO_2 absorption process in amine solutions, the effect of temperature on its equilibrium concentration was investigated. Figure 7(a) shows the equilibrium concentration of $RNHCOO^-$ as a function of CO_2 loading at different temperatures, and Figure 7(b) is the derived first-order difference curve. As can be seen, $RNHCOO^-$ concentration curves in Figure 7(a) all present a parabolic relationship in the investigated temperature range. $RNHCOO^-$ equilibrium concentration increases with CO_2 loading in regions I and II, whereas decreases in regions III and IV. The increasing rate of $RNHCOO^-$ concentration in regions I and II shows a distinct decline with increasing temperature, as illustrated in Figure 7(b). The lower $RNHCOO^-$ equilibrium concentration at higher temperatures with CO_2 loading lower than 0.5 CO_2/mol MEA in Figure 7(a) also illustrates this. As we discussed above, the dominant process in regions I and II is $RNHCOO^-$ formation reaction (Reaction (3)), which is an exothermic process. According to Le Chatelier's principle (the equilibrium law), increasing temperature causes equilibrium to shift to the left side of Reaction (3), namely, the lower increasing rate of $RNHCOO^-$ concentration. In contrast, $RNHCOO^-$ consumption reaction (Reaction (8)) becomes dominant in regions III and IV, which is also an exothermic reaction because K_9 is negatively related with temperature as shown in Table 3. Therefore, the decreasing rates of $RNHCOO^-$ concentration become lower at higher temperatures in regions III and IV, as shown in Figure 7(b). Finally, $RNHCOO^-$ equilibrium concentration at higher temperatures exceeds that at lower temperatures at the point of CO_2 loading of 0.66 CO_2/mol MEA, as shown in Figure 7(a).

In addition, we also studied the effect of temperature on CO_2 bulk equilibrium concentration. As shown in Figure 8, the bulk CO_2 concentration is zero in regions I and II and gradually increases with CO_2 loading in regions III and IV. In the first two regions, CO_2 dissolved in MEA solution is all converted into carbamate by MEA. Whereas when CO_2 loading is higher than 0.5 CO_2/mol MEA (regions III and IV), MEA is completely consumed. The dissolved CO_2 can be converted into HCO_3^- by the hydrolysis reaction or exists in the form of molecular state. As CO_2 hydrolysis is an

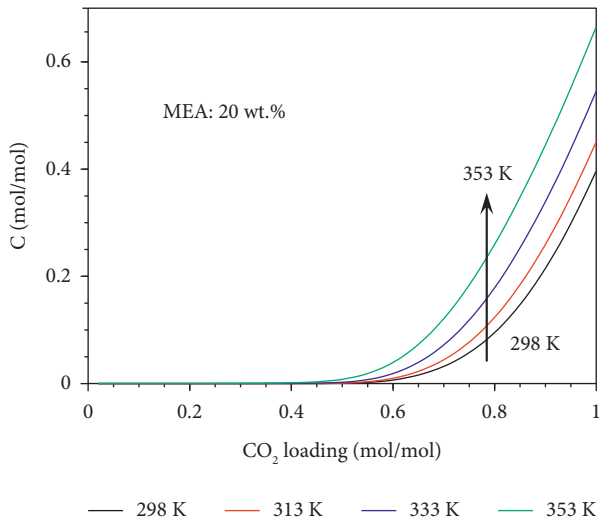

Figure 8: Bulk CO_2 concentrations at different temperatures as a function of CO_2 loading.

exothermic reaction, it consequently results in more CO_2 existing in the form of molecular state at higher temperature, as illustrated in Figure 8. Furthermore, as the interfacial concentration of CO_2 (equilibrium to the gas phase) will decrease with the increase in temperature at fixed CO_2 partial pressure, the bulk CO_2 concentration (equals to the interfacial concentration at equilibrium) also decreases at higher temperature. From Figure 8, a higher bulk CO_2 concentration in the curve of higher temperatures corresponds to a lower CO_2 loading. Therefore, it can be concluded that CO_2 solubility will decrease with increasing temperature, which is in agreement with the experimental results presented in Section 3.2.

4. Conclusion

This work has systematically investigated CO_2 absorption equilibrium in MEA aqueous solution by experimental measurement combined with thermodynamic model. The data of CO_2 solubility in MEA were measured at 298, 313, 333, and 353 K over a CO_2 partial pressure range of 34.5 to 78.0 kPa. C_{out}/C_{in} is close to zero in the first 35 minutes of the absorption process at 298 K, and then increases rapidly. The absorption curve moves leftwards with increasing temperature, indicating a faster saturation. A modified Kent-Eisenberg model was developed using the measured solubility data based on the Kent-Eisenberg model framework. The obtained thermodynamic model shows a good prediction of the species distribution of 20 wt.% MEA system under different CO_2 loadings.

In the first attempts to analyze the absorption process, a difference curve of the equilibrium concentrations of liquid-phase species as a function of CO_2 loading has been used. According to the change of reaction processes, CO_2 absorption process has been divided into four regions with CO_2 loadings ranging from 0 to 1. CO_2 dissolved in the aqueous MEA solution is all converted into carbamate in the first region. The difference value of $RNHCOO^-$ concentration decreases significantly in the second region. The difference value of $RNHCOO^-$ begins to be negative, namely, the equilibrium concentration of $RNHCOO^-$ begins to decrease in the third region. Only the consumption reaction of $RNHCOO^-$ and CO_2 hydrolysis reaction take place in the fourth region. Furthermore, based on the characteristics of each region, we propose that further kinetic study for measuring reaction rates and kinetic constants should be conducted in the first region, whereas measuring of mass transfer rates could be conducted in the first three regions. The innovative division of CO_2 absorption into four regions contributes to a deeper understanding of the process, as well as providing guidance for further kinetic studies. In addition, this novel method can be further extended to more CO_2 absorption processes utilizing different absorbents at various conditions. The CO_2 absorption processes using microreactors can also be easily applied to a larger-scale reaction by simply numbering-up.

Nomenclature

α: CO_2 loading;
C: Concentration, mol/m^3;
H: Henry's law constant, $kPa/(kmol/m^3)$;
K: Equilibrium constant;
n: Mole number, mol;
p: Pressure, Pa;
Q: Gas flow, m^3/s;
R: Gas constant, J/(K mol);
t: Time, s;
T: Temperature, K;
in: Inlet;
abs: Absorption;
exp: Experimental;
cal: Calculative;
gas: Gas phase;
L: Liquid phase;
t: Total.

Data Availability

All data used to support the findings of this study are currently under embargo while the research findings are commercialized. Requests for data, 12 months after publication of this article, will be considered by the corresponding author.

Conflicts of Interest

The authors declare that they have no conflicts of interest.

Acknowledgments

The authors gratefully acknowledge the financial supports for this project from the China State Construction Engineering Corp. (CSCEC-2021-Z-51 and CSCEC-PT-007-02), the China Construction Industrial & Energy Engineering Group Co. Ltd. (AZ-2020-02), Nanjing Municipal Commission of Urban-Rural Development (Ks2253), General Project of Natural Science Research in Colleges and Universities of Jiangsu Province (No. 21KJB530009), and Opening Fund of National & Local Joint Engineering Research Center for Deep Utilization Technology of Rock-Salt Resource (Grant no. SF202007).

References

[1] H. Herzog, B. Eliasson, and O. Kaarstad, "Capturing greenhouse gases," *Scientific American*, vol. 282, no. 2, pp. 72–79, 2000.

[2] Z. Liang, K. Fu, R. Idem, and P. Tontiwachwuthikul, "Review on current advances, future challenges and consideration issues for post-combustion CO_2 capture using amine-based absorbents," *Chinese Journal of Chemical Engineering*, vol. 24, no. 2, pp. 278–288, 2016.

[3] Z. H. Liang, W. Rongwong, H. Liu et al., "Recent progress and new developments in post-combustion carbon-capture technology with amine based solvents," *International Journal of Greenhouse Gas Control*, vol. 40, pp. 26–54, 2015.

[4] D. Aaron and C. Tsouris, "Separation of CO_2 from flue gas: a Review," *Separation Science and Technology*, vol. 40, no. 1-3, pp. 321–348, 2005.

[5] C. Yao, K. Zhu, Y. Liu, H. Liu, F. Jiao, and G. Chen, "Intensified CO_2 absorption in a microchannel reactor under elevated pressures," *Chemical Engineering Journal*, vol. 319, pp. 179–190, 2017.

[6] A. Uddin, F. X. Qin, D. Estevez, and H. X. Peng, "Vertical interface augmented tunability of scattering spectra in ferromagnetic microwire/silicone rubber metacomposites," *EPJ Applied Metamaterials*, vol. 8, p. 10, 2021.

[7] J. Tan, H. W. Shao, J. H. Xu, L. Du, and G. S. Luo, "Mixture absorption system of monoethanolamine triethylene glycol for CO_2 capture," *Industrial & Engineering Chemistry Research*, vol. 50, no. 7, pp. 3966–3976, 2011.

[8] C. Zheng, J. Tan, Y. J. Wang, and G. S. Luo, "CO_2 solubility in a mixture absorption system of 2-amino-2-methyl-1-propanol with glycol," *Industrial & Engineering Chemistry Research*, vol. 51, no. 34, pp. 11236–11244, 2012.

[9] C. Zheng, J. Tan, Y. J. Wang, and G. S. Luo, "CO_2 solubility in a mixture absorption system of 2-amino-2-methyl-1-propanol with ethylene glycol," *Industrial & Engineering Chemistry Research*, vol. 52, no. 34, pp. 12247–12252, 2013.

[10] C. Ye, M. Dang, C. Yao, G. Chen, and Q. Yuan, "Process analysis on CO_2 absorption by monoethanolamine solutions in microchannel reactors," *Chemical Engineering Journal*, vol. 225, pp. 120–127, 2013.

[11] C. Ye, G. Chen, and Q. Yuan, "Process characteristics of CO_2 absorption by aqueous monoethanolamine in a microchannel reactor," *Chinese Journal of Chemical Engineering*, vol. 20, no. 1, pp. 111–119, 2012.

[12] E. T. Hessen, T. Haug-Warberg, and H. F. Svendsen, "The refined e-NRTL model applied to CO_2–H_2O–alkanolamine systems,," *Chemical Engineering Science*, vol. 65, no. 11, pp. 3638–3648, 2010.

[13] S. Lange, S. Moioli, and L. A. Pellegrini, "Vapor-liquid equilibrium and enthalpy of absorption of the CO_2-MEA-H_2O System," *Chemical Engineering Transactions*, vol. 43, pp. 1975–1980, 2015.

[14] S. Freguia and G. T. Rochelle, "Modeling of CO_2 capture by aqueous monoethanolamine," *AIChE Journal*, vol. 49, no. 7, pp. 1676–1686, 2003.

[15] S. Ziaii, G. T. Rochelle, and T. F. Edgar, "Dynamic modeling to minimize energy use for CO_2 capture in power plants by aqueous monoethanolamine," *Industrial & Engineering Chemistry Research*, vol. 48, no. 13, pp. 6105–6111, 2009.

[16] S. Moioli, T. Nagy, S. Lange, L. A. Pellegrini, and P. Mizsey, "Simulation model evaluation of CO_2 capture by aqueous MEA scrubbing for heat requirement analyses," *Energy Procedia*, vol. 114, pp. 1558–1566, 2017.

[17] S. Mouhoubi, L. Dubois, P. Loldrup Fosbøl, G. De Weireld, and D. Thomas, "Thermodynamic modeling of CO_2 absorption in aqueous solutions of N, N-diethylethanolamine (DEEA) and N-methyl-1, 3-propanediamine (MAPA) and their mixtures for carbon capture process simulation," *Chemical Engineering Research and Design*, vol. 158, pp. 46–63, 2020.

[18] S. Ma'mun, K. Sukirman, D. Kuriawan et al., "Experimental determination of monoethanolamine protonation constant and its temperature dependency," *MATEC Web of Conferences*, vol. 101, p. 02001, 2017.

[19] U. E. Aronu, S. Gondal, E. T. Hessen et al., "Solubility of CO_2 in 15, 30, 45 and 60 mass% MEA from 40 to 120°C and model representation using the extended UNIQUAC framework," *Chemical Engineering Science*, vol. 66, no. 24, pp. 6393–6406, 2011.

[20] M. S. Ojala, N. Ferrer Serrano, P. Uusi-Kyyny, and V. Alopaeus, "Comparative study: absorption enthalpy of carbon dioxide into aqueous diisopropanolamine and monoethanolamine solutions and densities of the carbonated amine solutions," *Fluid Phase Equilibria*, vol. 376, pp. 85–95, 2014.

[21] M. Wagner, I. von Harbou, J. Kim, I. Ermatchkova, G. Maurer, and H. Hasse, "Solubility of carbon dioxide in aqueous solutions of monoethanolamine in the low and high gas loading regions," *Journal of Chemical & Engineering Data*, vol. 58, no. 4, pp. 883–895, 2013.

[22] Y. Zhang, H. Chen, C. C. Chen, J. M. Plaza, R. Dugas, and G. T. Rochelle, "Rate-based process modeling Study of CO_2 capture with aqueous monoethanolamine solution," *Industrial & Engineering Chemistry Research*, vol. 48, no. 20, pp. 9233–9246, 2009.

[23] J. P. Jakobsen, J. Krane, and H. F. Svendsen, "Liquid-phase composition determination in CO_2–H_2O–alkanolamine systems: an NMR study," *Industrial & Engineering Chemistry Research*, vol. 44, no. 26, pp. 9894–9903, 2005.

[24] W. Böttinger, M. Maiwald, and H. Hasse, "Online NMR spectroscopic study of species distribution in MEA–H_2O–CO_2 and DEA–H_2O–CO_2 Fluid Phase Equilibria," *Fluid Phase Equilibria*, vol. 263, no. 2, pp. 131–143, 2008.

[25] M. K. Wong, A. M. Shariff, and M. A. Bustam, "Raman spectroscopic study on the equilibrium of carbon dioxide in aqueous monoethanolamine," *RSC Advances*, vol. 6, no. 13, pp. 10816–10823, 2016.

[26] M. Xiao, D. Cui, L. Y. Zou, Q. Yang, H. X. Gao, and Z. W. Liang, "Experimental and modeling studies of bicarbonate forming amines for CO_2 capture by NMR spectroscopy and VLE," *Separation and Purification Technology*, vol. 234, p. 116097, 2020.

[27] S. H. Park, K. B. Lee, J. C. Hyun, and S. H. Kim, "Correlation and prediction of the solubility of carbon dioxide in aqueous alkanolamine and mixed alkanolamine solutions," *Industrial & Engineering Chemistry Research*, vol. 41, no. 6, pp. 1658–1665, 2002.

[28] R. L. Kent and B. Eisenberg, "Better data for amine treating," *Hydrocarbon Processing*, vol. 55, pp. 87–90, 1976.

[29] S. P. Balaji, S. Gangarapu, M. Ramdin et al., "Simulating the reactions of CO_2 in aaqueous monoethanolamine solution by reaction ensemble Monte Carlo using the continuous fractional component method," *Journal of Chemical Theory and Computation*, vol. 11, no. 6, pp. 2661–2669, 2015.

[30] S. M. Li, G. W. Kang, and J. Chen, "Measurement and thermodynamic modeling for CO_2 solubility in the N-(2-

hydroxyethyl) piperazine," *Frontiers in Energy Research*, vol. 9, p. 11, 2021.

[31] T. Neumann, J. Poplsteinova Jakobsen, M. Thol, and R. Span, "A new model combining Helmholtz energy equations of state with excess Gibbs energy models to describe reactive mixtures,," *Chemical Engineering Science*, vol. 252, p. 117261, 2022.

[32] M. Caplow, "Kinetics of carbamate formation and breakdown," *Journal of the American Chemical Society*, vol. 90, no. 24, pp. 6795–6803, 1968.

[33] A. Aboudheir, P. Tontiwachwuthikul, A. Chakma, and R. Idem, "Kinetics of the reactive absorption of carbon dioxide in high CO_2-loaded, concentrated aqueous monoethanolamine solutions," *Chemical Engineering Science*, vol. 58, no. 23-24, pp. 5195–5210, 2003.

[34] P. Danckwerts, "The reaction of CO_2 with ethanolamines," *Chemical Engineering Science*, vol. 34, no. 4, pp. 443–446, 1979.

[35] R. Oktavian, M. Taha, and M.-J. Lee, "Experimental and computational study of CO_2 storage and sequestration with aqueous 2-amino-2-hydroxymethyl-1,3-propanediol (TRIS) solutions," *Journal of Physical Chemistry A*, vol. 118, pp. 11572–11582, 2014.

[36] Y. C. Chang, R. B. Leron, and M. H. Li, "Equilibrium solubility of carbon dioxide in aqueous solutions of (diethylenetriamine+piperazine)," *The Journal of Chemical Thermodynamics*, vol. 64, pp. 106–113, 2013.

[37] Y. H. Hsu, R. B. Leron, and M. H. Li, "Solubility of carbon dioxide in aqueous mixtures of (reline+monoethanolamine) at T=(313.2 to 353.2)K," *The Journal of Chemical Thermodynamics*, vol. 72, pp. 94–99, 2014.

[38] D. Tong, G. C. Maitland, M. J. P. Trusler, and P. S. Fennell, "Solubility of carbon dioxide in aqueous blends of 2-amino-2-methyl-1-propanol and piperazine," *Chemical Engineering Science*, vol. 101, pp. 851–864, 2013.

[39] T. C. Tsai, J. J. Ko, H. M. Wang, C. Y. Lin, and M. H. Li, "Solubility of nitrous oxide in alkanolamine aqueous solutions," *Journal of Chemical & Engineering Data*, vol. 45, no. 2, pp. 341–347, 2000.

[40] W.-J. Choi, B.-M. Min, J.-B. Seo, S.-W. Park, and K.-J. Oh, "Effect of ammonia on the absorption kinetics of carbon dioxide into aqueous 2-amino-2-methyl-1-propanol solutions," *Industrial & Engineering Chemistry Research*, vol. 48, no. 8, pp. 4022–4029, 2009.

[41] M. Z. Haji-Sulaiman, M. K. Aroua, and A. Benamor, "Analysis of equilibrium data of CO_2 in aqueous solutions of diethanolamine (DEA), methyldiethanolamine (MDEA) and their mixtures using the modified Kent Eisenberg model," *Chemical Engineering Research and Design*, vol. 76, no. 8, pp. 961–968, 1998.

[42] Y. E. Kim, J. A. Lim, S. K. Jeong, Y. I. Yoon, S. T. Bae, and S. C. Nam, "Comparison of carbon dioxide absorption in aqueous MEA, DEA, TEA, and AMP solutions," *Bulletin of the Korean Chemical Society*, vol. 34, no. 3, pp. 783–787, 2013.

[43] J. I. Lee, F. D. Otto, and A. E. Mather, "Equilibrium between carbon dioxide and aqueous monoethanolamine solutions," *Journal of Applied Chemistry and Biotechnology*, vol. 26, no. 1, pp. 541–549, 2007.

[44] M. C. Simoes, K. J. Hughes, D. B. Ingham, L. Ma, and M. Pourkashanian, "Predicting speciation of ammonia, monoethanolamine, and diethanolamine using only ionic radius and ionic charge," *Industrial & Engineering Chemistry Research*, vol. 57, no. 6, pp. 2346–2352, 2018.